
Towards Better Long-range Time Series Forecasting using Generative Forecasting

Shiyu Liu, Rohan Ghosh, Mehul Motani
Department of Electrical and Computing Engineering
National University of Singapore
shiyu_liu@u.nus.edu, lsirg, motani@nus.edu.sg

Abstract

Long-range time series forecasting is usually based on one of two existing forecasting strategies: Direct Forecasting and Iterative Forecasting, where the former provides low bias, high variance forecasts and the latter leads to low variance, high bias forecasts. In this paper, we propose a new forecasting strategy called Generative Forecasting (GenF), which generates synthetic data for the next few time steps and then makes long-range forecasts based on generated and observed data. We theoretically prove that GenF is able to better balance the forecasting variance and bias, leading to a much smaller forecasting error. We implement GenF via three components: (i) a novel conditional Wasserstein Generative Adversarial Network (GAN) based generator for synthetic time series data generation, called CWGAN-TS. (ii) a transformer based predictor, which makes long-range predictions using both generated and observed data. (iii) an information theoretic clustering algorithm to improve the training of both the CWGAN-TS and the transformer based predictor. The experimental results on five public datasets demonstrate that GenF significantly outperforms a diverse range of state-of-the-art benchmarks and classical approaches. Specifically, we find a 5% - 11% improvement in predictive performance (mean absolute error) while having a 15% - 50% reduction in parameters compared to the benchmarks. Lastly, we conduct an ablation study to demonstrate the effectiveness of the components comprising GenF.

1 Introduction

Accurate forecasting of time series data is an important problem in many sectors, such as energy, finance and healthcare [33, 25, 41, 35, 2, 3]. In terms of prediction horizon, long-range forecasting (also called multi-step ahead forecasting) is often preferred than short-range forecasting (i.e., few time steps ahead) as it allows more time for early intervention and planning opportunities [49, 24, 32, 6, 23]. As an example, long-range forecasting of patient’s vital signs effectively gives clinicians more time to take actions and may reduce the occurrence of potential adverse events [7, 17, 49].

To perform long-range forecasting, there are two forecasting strategies: Direct Forecasting (DF) and Iterative Forecasting (IF). As the name suggests, DF directly makes predictions N time steps ahead, but the forecasting performance tends to decrease (i.e., variance increases) as N grows [27]. In IF, the previous predictions are used as part of the input to recursively make predictions for the next time step. However, the predictions made in such a recursive and supervised manner is susceptible to error propagation, resulting in degraded forecasting performance (i.e., bias increases) as N grows [39, 37].

In this paper, we improve the performance of long-range time series forecasting by proposing a new forecasting strategy. The contributions of our work are summarized as follows.

1. We propose a new forecasting strategy called Generative Forecasting (GenF), which generates synthetic data for the next few time steps and then makes long-range predictions based on generated and observed data. Theoretically, we prove that the proposed GenF is able to better balance the forecasting bias and variance, leading to a smaller forecasting error.
2. We implement GenF via three components: (i) a new conditional Wasserstein Generative Adversarial Network (GAN) [1, 29, 14, 13] based generator for synthetic time series data generation called CWGAN-TS. (ii) a transformer based predictor, which makes long-range predictions using both generated and observed data. (iii) a information theoretic clustering (ITC) algorithm to improve the training of both the CWGAN-TS and the transformer based predictor.
3. We conduct experiments on five public time series datasets and the experimental results demonstrate that GenF significantly outperforms a diverse range of state-of-the-art (SOTA) benchmarks and classical approaches. Specifically, we find a 5% - 11% improvement in predictive performance while having a 15% - 50% reduction in parameters compared to the SOTA benchmarks.
4. We conduct an ablation study to demonstrate the effectiveness of each component comprising GenF from the perspective of synthetic data generation and forecasting performance.

2 Background on Time Series Forecasting

Problem definition. Suppose we have an observation window containing multivariate observations for past M time steps $\{X_1, X_2, \dots, X_M \mid X_i \in \mathbb{R}^K\}$, where M is the observation window length, K is the number of features per observation and X_i is the observation at time step i (see Fig.1). The task of time series forecasting is to find an approach to map past observations to the future value, i.e., $\{X_1, X_2, \dots, X_M\} \rightarrow \bar{X}_{M+N}$. We note that N is the prediction horizon, indicating we plan to make predictions N time steps ahead (i.e., at time step $M+N$ in Fig. 1). Next, in Section 2.1, we discuss related work and the application of GAN-based models. In Section 2.2, we shortlist two classical models and five SOTA baselines for performance comparison.

2.1 Related Work

The example of early methods using neural networks to perform long-range forecasting is [31] which proposed a group of networks to make predictions at different time steps. Along the way, several works attempt to improve the long-range forecasting by proposing new architectures. For example, [48] proposed a Long Short-Term Memory (LSTM) [15] based Tensor-Train Recurrent Neural Network as a module for sequence-to-sequence framework [36], called TLSTM. [42] proposed an autoregressive recurrent network called DeepAR to provide probabilistic forecasts. [22] proposed a Long- and Short-term Time-series network (LSTNet) which incorporates with an attention-based layer and autoregressive models. More recently, transformer based models have shown superior performance in capturing long-range dependency than recurrent networks. Several recent works aim to improve the transformer by simplifying its complexity. As an example, LogSparse [24] and Reformer [20] use heuristics to reduce the complexity of self-attention mechanism from $\mathcal{O}(n^2)$ to $\mathcal{O}(n \log n)$, where n is the sequence length. Moreover, Informer [49] aimed to further reduce the complexity via ProbSparse and distilling operations. In terms of the forecasting strategy, all these methods can be classified into two main classes: direct forecasting and iterative forecasting.

In **direct forecasting**, the model f is trained to directly make predictions for the prediction horizon N , i.e., $\bar{X}_{M+N} = f(X_1, \dots, X_M)$ (see the illustration Fig. 1). The advantage is that the models trained for different values of N are independent and hence, immune to error propagation. However, as N grows, DF tends to provide predictions with low bias but high variance [39]. This can be seen by considering an example where the best forecast is a linear trend. In this case, DF may yield a broken curve as it does not leverage the dependencies of synthetic data [4].

In **iterative forecasting**, the model is trained to make predictions for the next time step only i.e., $\bar{X}_{M+1} = f(X_1, \dots, X_M)$ (see Fig. 1). The same model will be used over and over again and previous predictions are used together with the past observations to make predictions for the next time step (e.g., $\bar{X}_{M+2} = f(X_2, \dots, X_M, \bar{X}_{M+1})$). This process is recursively repeated to make predictions for next N time steps. The previous predictions can be considered as synthetic data with a synthetic window length = $N-1$. However, the synthetic data generated in such a supervised and recursive manner is susceptible to error propagation, i.e., a small error in the current prediction becomes larger in subsequent predictions, leading to low variance but high bias predictions [34]. Based on IF, to address the issue of error propagation, RECTIFY [38] rectifies the synthetic data to

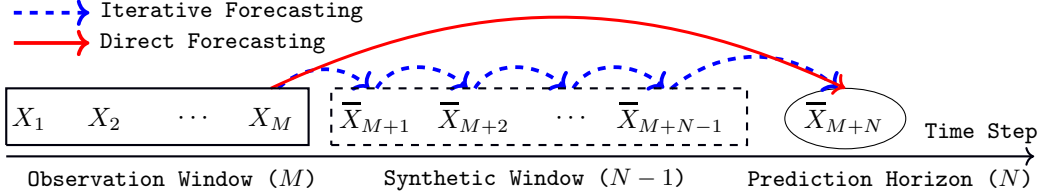


Figure 1: Direct/Iterative Forecasting via Observation/Synthetic Window and Prediction Horizon.

be unbiased and Seq2Seq based models [36] extends the decoder by adding more sequential models and each sequential model is trained for a specific prediction horizon with different parameters.

Recently, GAN based networks have demonstrated promising results in many generative tasks. The first GAN applied to time series data was C-RNN-GAN [30] which used LSTM as the generator and discriminator. Along the way, many works have explored generating synthetic data to address various problems. As an example, [12] used synthetic data augmentation to improve the classification results, and [Joon2019time proposed TimeGAN which trains predictive models to perform one-step ahead forecasting. However, to the best of our knowledge, the use of synthetic data generated by the GAN based networks to improve long-range forecasting remains largely unexplored.

2.2 Benchmark Methods

We shortlist five SOTA baselines discussed above: **(i) TLSTM** (seq2seq based model), **(ii) LSTNet** (attention based model), **(iii) DeepAR** (autoregressive based model), **(iv) LogSparse** (transformer based model) and **(v) Informer** (transformer based model) for comparison as they are reported to provide outstanding long-range forecasting performance [22, 49]. Moreover, the authors of these methods have provided clear and concise source code, allowing us to correctly implement and tune these algorithms. In addition, two classical time series forecasting approaches: **(i) LSTM and (ii) Autoregressive Integrated Moving Average (ARIMA)** [5] are examined for comparison as well.

3 Generative Forecasting (GenF)

We first introduce the idea of GenF in Section 3.1. Next, in Section 3.2, we theoretically prove that the proposed GenF is able to better balance the forecasting variance and bias, leading to a smaller forecasting error. Lastly, in Section 3.3, we detail the implementation of GenF.

3.1 Idea of GenF

To improve long-range time series forecasting, we develop an approach called Generative Forecasting (GenF), which consists of two steps (see our illustration in Fig. 2):

1. **Synthetic Data Generation:** GenF first generates synthetic data for next L time steps (i.e., $\tilde{X}_{M+1}, \dots, \tilde{X}_{M+L}$) conditioned on the past M observations.
2. **Long-range Prediction:** GenF concatenates the past observations (X_1, \dots, X_M) with the generated synthetic data ($\tilde{X}_{M+1}, \dots, \tilde{X}_{M+L}$) and keeps a window size of M by dropping the oldest observations, resulting in a sequence of $(X_{L+1}, \dots, X_M, \tilde{X}_{M+1}, \dots, \tilde{X}_{M+L})$. Finally, GenF makes long-range predictions for time step $M + N$ using $(X_{L+1}, \dots, X_M, \tilde{X}_{M+1}, \dots, \tilde{X}_{M+L})$ as input.

The **key difference** with DF and IF is that GenF leverages synthetic data to shorten the effective prediction horizon and has a flexible synthetic window length of L (see Fig. 2)), respectively. Unlike IF of which the synthetic window length depends on the prediction horizon, the synthetic window length L of GenF does not depend on the prediction horizon and is flexible. Adjusting the value of L is a trade-off between forecasting variance and bias. A large value of L brings GenF close to iterative forecasting, while a small value of L brings GenF close to direct forecasting.

3.2 Theoretical Results

In this section, we provide some theoretical insights into the behavior of forecasting error for the proposed GenF approach. In order to do so, we first undertake a bias-variance based approach for approximating the forecasting errors. Then, we estimate the variance of the low-bias direct forecasting step and the bias of the low-variance iterative forecasting step. Subsequently, we provide a theoretical result that bounds the forecasting error in terms of the bias and variance of the iterative

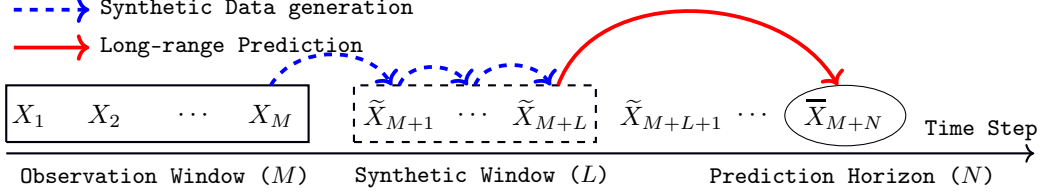


Figure 2: Illustration of GenF via Observation/Synthetic Window and Prediction Horizon.

and direct forecasting steps, respectively. Finally, we show that under certain conditions, the proposed GenF will yield much better performance. The proofs of the results given below are provided in the Appendix.

Let $Y = \{X_1, \dots, X_M\}$ be the past observations and $u_{M+N} = \mathbb{E}[X_{M+N}|Y]$ be the conditional expectation of N -step ahead observation. Let $f(Y, \theta, N)$ be the N -step ahead forecast using Y as the input with parameter $\theta \in \Theta$, where Θ represents the set of all possible trained parameter configurations from the dataset instances from the underlying data distribution. The Mean Squared Error (MSE) of a given strategy at prediction horizon N can be decomposed as follows [37].

$$\text{MSE}_N = \underbrace{\mathbb{E}_Y[(X_{M+N} - u_{M+N})^2|Y]}_{\text{Noise, } Z(N)} + \underbrace{\mathbb{E}_Y[(u_{M+N} - \mathbb{E}_\Theta[f(Y, \theta, N)])^2]}_{\text{Bias, } B(N)} + \underbrace{\mathbb{E}_{Y, \Theta}[(f(Y, \theta, N) - \mathbb{E}_\Theta[f(Y, \theta, N)])^2]}_{\text{Variance, } V(N)}. \quad (1)$$

The first term $Z(N)$ in (1) is irreducible noise, which does not depend on the forecasting strategy used. The second term $B(N)$ is the forecasting bias and the third term $V(N)$ is the forecasting variance. Both $B(N)$ and $V(N)$ depend on the employed forecasting strategy and tend to grow with the prediction horizon N . The ideal configuration is to have a low bias and a low variance. However, this is never achieved in practice as decreasing bias will increase the variance and vice versa. Hence, a good forecasting strategy is to better balance bias and variance, so as to obtain the smallest MSE.

Proposition 1. *Let S be the sum of bias and variance terms, we have $S_{dir} = B_{dir}(N) + V_{dir}(N)$ for direct forecasting and $S_{iter} = B_{iter}(N) + V_{iter}(N)$ for iterative forecasting. For GenF, let $Y_{M-L} = \{X_{L+1}, \dots, X_M\}$ and $Y_L = \{X_{M+1}, \dots, X_{M+L}\}$ be the past observations and let $\tilde{Y}_L = \{\tilde{X}_{M+1}, \dots, \tilde{X}_{M+L}\}$ be the generated synthetic data for the next L time steps. Let $\gamma(\theta, N - L) = f(\{Y_{M-L}, \tilde{Y}_L\}, \theta, N - L) - f(\{Y_{M-L}, Y_L\}, \theta, N - L)$. We then have,*

$$S_{GenF} = \underbrace{B_{iter}(L) + V_{iter}(L)}_{\text{Iterative Forecasting}} + \underbrace{B_{dir}(N - L) + V_{dir}(N - L) + \mathbb{E}_{\theta \sim \Theta}[\gamma(\theta, N - L)^2]}_{\text{Direct Forecasting}}. \quad (2)$$

The proposition yields the joint bias and variance of the proposed GenF method. Using this breakdown, the following Theorem and Corollary provide error bounds using this framework.

Theorem 1. *We consider the direct forecasting with parameters θ_D , iterative forecasting with parameters θ_I , and the proposed GenF in Proposition (1). Assume that the ground truth realization of the forecasting process can be modelled by some θ_D^* and θ_I^* , and after training, the estimated parameters follow $\theta_D \sim \mathcal{N}(\theta_D^*, \sigma_D^2)$ and $\theta_I \sim \mathcal{N}(\theta_I^*, \sigma_I^2)$. Assume that the iterative forecasting function is 2nd-order L_1, L_2 -Lipschitz continuous, and the direct forecasting function is first order Lipschitz continuous. Let us denote quadratic recurrence relations of the form $b_\alpha(k + 1) = b_\alpha(k)(L_1 + 1 + b_\alpha(k)L_2)$, where $b_\alpha(1) = \alpha\sigma_I^2$, for any $\alpha \geq 0$. Assume that iterative forecasting has zero variance and direct forecasting has zero bias. Then, for some constants $\beta_0, \beta_1, \beta_2 \geq 0$, which represent the Lipschitz constants of the direct forecasting function, we have $S_{dir} \leq U_{dir}$, $S_{iter} \leq U_{iter}$ and $S_{GenF} \leq U_{GenF}$, where $U_{dir} = (N - 1)\beta_1 + \sigma_D^2\beta_2$, $U_{iter} = b_\alpha(N)^2$, and $U_{GenF} = b_\alpha(L)^2(\beta_0) + (N - L - 1)\beta_1 + \sigma_D^2\beta_2$. The quantities α and $\beta_0, \beta_1, \beta_2$ depend on the iterative and direct forecasting functions respectively.*

Corollary 1. *U_{dir} , U_{iter} and U_{GenF} are as defined in Theorem 1. When $\beta_0 < \min\{\beta_1/b_\alpha(1)^2, (b_\alpha(N)^2 - \sigma_D^2\beta_2)/b_\alpha(N - 1)^2\}$, we have that $U_{GenF} < U_{iter}$ and $U_{GenF} < U_{dir}$, for some $0 < L < N$. Furthermore, when $(N - 1)\beta_1 + \sigma_D^2\beta_2 \approx b_\alpha(N)^2$, we have $U_{GenF} < U_{iter}$ and $U_{GenF} < U_{dir}$, for any choice of $0 < L < N$.*

Remark 1. *Theorem 1 provides upper bounds on the sum of bias and variance terms, and Corollary 1 provides the conditions under which the upper bounds for GenF are provably lower. One of the possible scenarios these conditions are satisfied is when the iterative forecaster has low single-horizon bias (i.e., $b_\alpha(1)$), and a large prediction horizon N . Corollary 1 suggests that under certain*

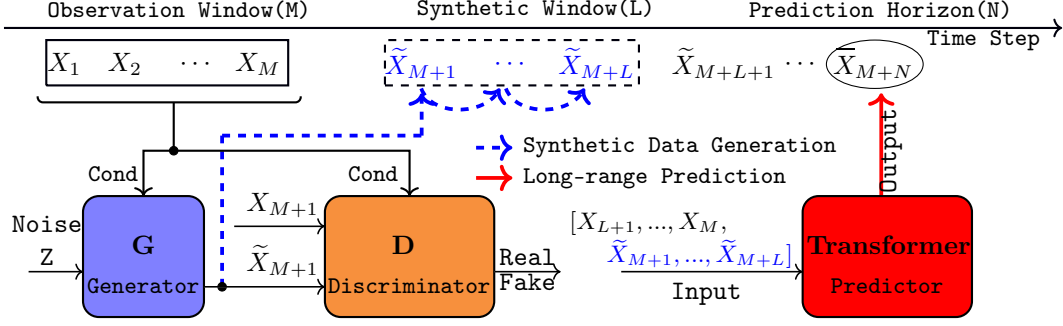


Figure 3: Implementation of GenF (Left: CWGAN-TS; Right: Transformer based Predictor).

conditions, GenF can provide potentially smaller MSE, which is verified in our experiments in Section 4.3. Corollary 1 also gives conditions under which GenF yields a smaller upper bound on error for any $0 < L < N$.

3.3 Implementation of GenF

We now detail the implementation of GenF via three components as follows.

1) CWGAN-TS: Synthetic Data Generation. For the iterative forecasting part (i.e., $B_{iter}(L) + V_{iter}(L)$) of GenF in (6), the bias term ($B_{iter}(L)$) tends to be more dominant due to the nature of iterative forecasting. Therefore, we should select a low bias model for the iterative forecasting part in (6), so as to obtain a smaller MSE. A recent work [10] evaluates the generative bias of a diverse range of models and their results suggest that GAN based models tend to have a relatively lower generative bias than other models studied (e.g., VAE). Similar results are reported in [16] as well. This motivates the use of a GAN based model in our proposed GenF for synthetic data generation.

We propose a Conditional Wasserstein GAN for synthetic time series data generation [1, 29, 14], called CWGAN-TS. The the unsupervised loss of CWGAN-TS is summarized as follows.

$$\mathcal{L}_U = \mathbb{E}_{\bar{X}_{M+1} \sim P_g} [D(\bar{X}_{M+1}|Y)] - \mathbb{E}_{X_{M+1} \sim P_r} [D(X_{M+1}|Y)] + \lambda \mathbb{E}_{\hat{X}_{M+1} \sim P_{\hat{X}}} [(\|\nabla_{\hat{X}} D(\hat{X}_{M+1}|Y)\|_2 - 1)^2], \quad (3)$$

where $Y = \{X_1, \dots, X_M\}$ is the condition, $X_{M+1} \sim P_r$ is the real data at time step $M + 1$, $\bar{X}_{M+1} \sim P_g$ is the generated data for time step $M + 1$ and $\hat{X}_{M+1} \sim P_{\hat{X}}$ is sampled from \bar{X}_{M+1} and X_{M+1} with ϵ uniformly sampled between 0 and 1, i.e., $\hat{X}_{M+1} = \epsilon \bar{X}_{M+1} + (1 - \epsilon) X_{M+1}$ with $0 \leq \epsilon \leq 1$. The first two terms in (3) correspond to Wasserstein distance which improves learning performance over the Jensen-Shannon divergence used in the original GAN. The third term is the gradient penalty, corresponding to the 1-Lipschitz constraint [14]. To control the generation of synthetic data, we apply two terms to CWGAN-TS during training: (i) the past observation Y as the condition. (ii) an additional supervised loss as follows.

$$\mathcal{L}_S = \mathcal{L}_U + \eta \|X_{M+1} - \bar{X}_{M+1}\|_2, \quad (4)$$

where η is a hyperparameter that balances the two losses. Importantly, this is, in addition to the unsupervised minmax game played over classification accuracy, the generator additionally minimizes the supervised loss. By combining the objectives in this manner, CWGAN-TS aims to generate accurate synthetic data while preserving the temporal dynamics between conditioning input and generated data. The loss function of CWGAN-TS is further evaluated via an ablation study.

2) Transformer: Long-range Prediction. Several recent works [24, 49, 46, 45, 11, 26, 40] have shown the great potential of transformer in time series forecasting. We briefly introduce its architecture here and refer interested readers to [43] for more details.

In the self-attention layer, a multi-head self-attention sublayer takes input \mathbf{Y} (i.e., time series data and its positioning vectors) and computes the attention function simultaneously using query matrices: $\mathbf{Q}_h = \mathbf{Y}\mathbf{W}_h^Q$, key matrices $\mathbf{K}_h = \mathbf{Y}\mathbf{W}_h^K$, and value matrices $\mathbf{V}_h = \mathbf{Y}\mathbf{W}_h^V$. Note that \mathbf{W}_h^Q , \mathbf{W}_h^K and \mathbf{W}_h^V are learnable parameters. The scaled dot-product attention computes a sequence of vector outputs:

$$\mathbf{O}_h = \text{Attention}(\mathbf{Q}_h, \mathbf{K}_h, \mathbf{V}_h) = \text{softmax}\left(\frac{\mathbf{Q}_h \mathbf{K}_h^T}{\sqrt{d_k}} \cdot \mathbf{M}\right) \mathbf{V}_h \quad (5)$$

where $\frac{1}{\sqrt{d_k}}$ is a scaled factor and \mathbf{M} is a mask matrix. In GenF, we concatenate \mathbf{O}_h ($h = 1, \dots, H$ and H is number of heads) and pass the concatenation through several fully connected layers before arriving at the final output. The architecture details can be found in Table 3 in the Appendix.

3) The ITC Algorithm. The datasets studied in this paper contain time series data for different patients, countries and so on. In the following, we refer to them as units. Since GenF contains two steps, synthetic data generation and long-range forecasting, it requires two independent datasets: datasets \mathbb{G} and \mathbb{P} to train the CWGAN-TS and the transformer based predictor, respectively. It is possible to randomly split the entire training dataset at unit level into datasets \mathbb{G} and \mathbb{P} , but the resulting datasets may not represent the entire training dataset well. We address this issue by suggesting an information theoretic clustering (ITC) algorithm based on Mutual Information (MI), denoted by $I(X; Y)$, which is a well-studied measure from information theory [8] that quantifies the dependency between random variables X and Y .

The ITC algorithm aims to select representative training subsets to better train the CWGAN-TS and the transformer based predictor. It consists of three steps: (i) Assign a score to each unit via the scoring function $J(P_i) = \sum_{P_j \in \mathbb{D}, P_j \neq P_i} I(P_i, P_j)$, where P_i refers to the candidate unit and $\mathbb{D} = \{P_1, P_2, \dots\}$ is the dataset containing all units. To estimate MI (i.e., $I(P_i, P_j)$), we use a nearest neighbor based approach called KSG estimator [21] as all features studied are continuous variables. (ii) Divide all units into γ groups based on the descending order of all scores, where γ is a tunable parameter. The units with similar scores will be grouped together and units within the same group tend to be highly dependent on each other. (iii) Randomly sample from each subgroup. This is equivalent to selecting representative units of each subgroup. Random proportional sampling from all groups gives a new training dataset \mathbb{G} and the remaining units form the new training dataset \mathbb{P} . In such a manner, we argue that we can select more representative units for better training.

4 Performance Evaluation

We summarize the dataset information in Section 4.1 and describe the experimental setup in Section 4.2. Next, in Section 4.3, we compare the performance of GenF to benchmark methods. Lastly, we conduct an ablation study to evaluate the effectiveness of our framework in Section 4.4.

4.1 Real-world Datasets

We shortlist five public time series datasets comprising different time series patterns (e.g., periodical, monotonic) and time intervals (e.g., hourly, daily, annual) from three popular domains (healthcare, environment and energy consumption). We summarize each dataset as follows.

1. The Vital Sign dataset from MIMIC-III [18], which contains 500 patients in the MIMIC-III Clinical database. For each patient, we extract 6 features: heart rate (bpm), respiratory rate, blood oxygen saturation (%), body temperature ($^{\circ}$ F), systolic and diastolic blood pressure (mmHg). The vital signs are recorded at a hourly interval over a duration of 144 hours on average.
2. The Multi-Site Air Quality dataset from UCI [9], which includes air pollutants data from 12 sites. For each site, we extract the hourly record of PM10, SO₂, NO₂, O₃, PM2.5 and CO. We note that all features are in units of $\mu\text{g}/\text{m}^3$ and each site has 35,000 records on average.
3. The World Energy Consumption dataset from World Bank [44], which contains data from 128 countries and each country contains three annual energy consumption indicators: electricity (kWh/capita), fossil fuel (% of total) and renewable energy (% of total) from 1971 to 2014.
4. The Greenhouse Gas dataset from UCI [9], which records the greenhouse gas concentrations (ppm) at 2921 locations. The data points are spaced 6 hours apart over a period of three months.
5. The Household Electricity Consumption dataset [28], which contains the cumulative daily electricity consumption (kWh) for 995 households over a duration of three years.

For each dataset, a small amount (i.e., less than 5%) of missing values are imputed using the last historical readings. Moreover, we scale all variables to [0,1] and reshape all scaled data via a sliding window, resulting in a dataset $\mathbb{D} \in \mathbb{R}^{S \times M \times K}$, where S is the number of samples, K is number of features and M is the observation window length.

4.2 Experiment Setup & Parameter Tuning

In the experiment, the dataset \mathbb{D} is randomly split into three subsets at unit level: training dataset $\mathbb{T} \in \mathbb{R}^{S_1 \times M \times K}$ (60%), test dataset $\mathbb{Q} \in \mathbb{R}^{S_2 \times M \times K}$ (20%) and validation dataset $\in \mathbb{R}^{S_3 \times M \times K}$

Prediction Horizon	t + 8		t + 12		t + 30		t + 60		
Metrics	MAE	sMAPE	MAE	sMAPE	MAE	sMAPE	MAE	sMAPE	
ARIMA	8.3±1.3	7.3±1.1	9.8±0.8	8.4±0.7	16.2±1.7	13.1±1.4	18.9±2.7	14.5±2.4	
LSTM	7.3±0.6	6.4±0.3	8.9±1.1	7.6±0.9	13.9±1.3	11.0±0.9	17.8±2.9	13.3±1.9	
SOTA	TLSTM	6.8±0.4	5.7±0.4	8.2±0.6	7.1±0.8	12.3±1.2	10.9±1.1	15.0±2.3	12.7±1.5
	LSTNet	6.9±0.6	5.8±0.4	8.2±0.7	7.0±0.7	12.0±1.3	10.6±1.3	14.2±2.6	11.5±0.9
	DeepAR	6.8±0.5	6.0±0.6	8.4±1.1	7.2±0.9	12.9±1.1	11.2±0.9	16.3±2.8	12.9±1.7
	Informer	6.5±0.4	5.3±0.5	7.9±0.7	6.6±0.7	11.8±1.5	10.1±1.4	14.1±2.7	11.5±1.6
	LogSparse	6.6±0.7	5.5±0.3	8.1±0.5	6.9±0.6	11.6±1.0	9.7±0.9	14.5±2.8	11.3±1.2
GenF-3 (Ours)	6.2±0.4	5.1±0.5	7.5±0.6	6.3±0.5	11.2±1.4	9.2±1.0	13.5±2.7	10.8±1.9	
GenF-6 (Ours)	6.3±0.4	5.2±0.3	7.4±0.7	6.2±0.6	10.7±1.1	8.9±0.9	12.6±2.5	10.2±1.4	

Table 1: Performance (MAE, sMAPE (%) \pm standard deviation over 5 runs) of **predicting blood pressure using Vital Sign dataset**. Similar performance trends are observed for the other four datasets (see Tables 4 - 7 in the Appendix). The X in GenF-X is the synthetic window length L .

(20%). We note that both GenF and the benchmark methods are trained using the training dataset \mathbb{T} , and the test dataset \mathbb{Q} is used to evaluate the performance. **To ensure fair comparison, we conduct grid search over all tunable hyper-parameters and possible configurations using the validation dataset.** We highlight that all methods share the same grid search range and step size. Specifically, some key parameters are tuned as follows. (i) the hidden state size of LSTM is tuned from 5 to 100 with step size of 5. (ii) the size of fully connected layers are tuned from 1 to 10 with step size of 1. (iii) the number of heads in multi-head self-attention layer are tuned from 1 to 10 with step size of 1.

We now provide a list of tuned parameters for predicting systolic blood pressure using the MIMIC-III Vital Signs dataset. In terms of the classical models: (i) ARIMA (2,0,1) is trained using the past M historical values of a single feature (e.g., systolic blood pressure). (ii) for the canonical transformer, it contains two encoder layers, two decoder layers and three heads in the multi-head self-attention layer. (iii) for LSTM, we stack two LSTM layers (each LSTM with hidden size of 10) and two fully connected layers (with size of 10 and 1, respectively). This LSTM based neural network is directly trained using training dataset \mathbb{T} for 1000 epochs using Adam [19] with a learning rate of 0.001, in batches of 64. As for the five SOTA methods, we refer to the source code released by their authors and some key parameters are as follows: LSTNet has a skip-length of 5 and a gradient clipping of 10, TLSTM uses a dropout of 0.1 and LogSparse uses a kernel size of 9 and an embedding size of 16. In terms of GenF, we use the LSTM and fully connected layer to implement the CWGAN-TS. The transformer based predictor consists of two decoder layers and two encoder layers, with three heads. For the detailed algorithm of GenF and other training details on five SOTA methods, we refer interested reader to Algorithm 1 and Table 3 in the Appendix. **Furthermore, we use Tesla V100 devices for our experiments, and the source code (including random seeds) will be released for reproducibility at the camera-ready stage.**

In the experiments, we compare the performance of GenF to two classical models and five SOTA methods. The Mean Squared Error (MSE) and Mean Absolute Error (MAE) are used to evaluate the performance, where the former captures both the variance and bias of the predictor, and the latter is useful to understand whether the size of the error is of concern or not. Furthermore, a scale invariant error metric called symmetric Mean Absolute Percentage Error (sMAPE) is also used. In Table 1, we show the performance of several variants of GenF (i.e., GenF-3, GenF-6), where the 'X' in GenF-X represents the value of the synthetic window length L .

4.3 Performance Comparison

(1) GenF VS SOTA Methods. In Table 1, we demonstrate that GenF greatly outperforms all methods studied for predicting blood pressure on the Vital Sign dataset. For example, the MAE of GenF-3 at $t + 8$ is 8.8% better than the classical seq2seq based method (TLSTM), 10.1% better than the attention based method (LSTNet), 5% better than the transformer based method (Informer). Interestingly, as the prediction horizon grows, generating more synthetic data could be helpful, leading to better forecasting performance. Specifically, comparing to the best performing benchmark, GenF-6 achieves an improvement of 7.7% at $t + 30$ and 10.6% at $t + 60$. Similar performance trends can be observed using the other four datasets described in Section 4.1 (see Tables 4 - 7 in the Appendix).

	DF	IF	GenF-2	GenF-4	GenF-6	GenF-8	GenF-10
$t + 8$	147 ± 7	153 ± 10	138 ± 9	134 ± 7	141 ± 9	–	–
$t + 12$	168 ± 11	177 ± 15	159 ± 13	156 ± 11	152 ± 13	157 ± 11	166 ± 10
$t + 30$	206 ± 19	221 ± 24	189 ± 17	185 ± 16	179 ± 19	188 ± 15	186 ± 16

Table 2: Performance (MSE \pm standard deviation over 5 runs) comparison between GenF with different lengths of synthetic window and DF/IF for predicting blood pressure on Vital Sign dataset.

(2) Complexity Comparison. We note that GenF is essentially a transformer based method as it uses a shallow transformer based predictor. When predicting the blood pressure, the parameter count for GenF and the other two transformer based SOTA methods are: (i) GenF: 9.0K (CWGAN-TS: 3K; Transformer based Predictor: 6K), (ii) Informer: 10.6K and (iii) LogSparse: 17.9K. GenF uses 15% and 50% less parameters than Informer and LogSparse, respectively, but has better performance than both. We note that these SOTA methods aim to better capture long-range dependencies with deep transformers. GenF achieves the same goal by extending the existing time series with synthetic data. As a result, our shallow transformer is able to achieve better performance than the deep transformers.

(3) Strategy Comparison: GenF VS DF/IF. In Table 2, we vary the length of synthetic window for GenF and compare its performance to DF and IF, where DF can be understood as GenF with synthetic window length of zero and IF can be considered as GenF with synthetic window length of $N - 1$ (i.e., N is the prediction horizon). We use the same canonical transformer to implement both GenF and DF/IF, so as to evaluate the forecasting strategy itself. The forecasting performance is measured using MSE to capture both variance and bias of the predictor. In Table 2, we observe that, for the three tasks conducted (i.e., $t + 8$, $t + 12$, $t + 30$), GenF tends to obtain the lowest MSE. As an example, the MSE of GenF-4 at $t + 8$ is 134, which is 8.8% and 12.4% lower than DF and IF, respectively. This verifies our theoretical results in Corollary 1 using experiments, namely that GenF is able to better balance the forecasting variance and bias, leading to a much smaller MSE.

4.4 Ablation Study

We now conduct an ablation study to demonstrate the effectiveness of key components in GenF. Specifically, we remove one component at a time in GenF and observe the impact on synthetic data generation and forecasting performance. We construct three variants of CWGAN-TS as follows: **(i) CWGAN-GP:** CWGAN-TS without the squared error penalty term in the loss function (4). **(ii) CWGAN-RS:** CWGAN-TS without the ITC algorithm, instead, the CWGAN-TS is trained with a randomly selected training subset. **(iii) GAN:** A conventional GAN [13] without considering the Wasserstein distance. More importantly, **the advantage of GAN loss** in generating synthetic data is demonstrated by comparing to LSTM.

(1) Experiment Setup. In the experiment of predicting heart rate on the Vital Sign dataset, we shortlist a unit called Subject ID 23 and show the observation window ($M = 20$), synthetic window ($L = 3$) and the prediction horizon ($N = 1, \dots, 5$) in Fig. 4. Specifically, in synthetic window, we show the synthetic data generated by CWGAN-TS, its three variants and two classical models (ARIMA and LSTM) up to $t = 23$. In the prediction horizon, we use the same predictor to evaluate the forecasting performance of all models by taking their past observations and the synthetic data ($t = 21$ to 23) as the input. As a comparison, we also show the true value (solid line). In Fig. 4, the values in parentheses are the MSE of the synthetic data generation and the forecasting performance, averaged over the synthetic window and prediction horizon, respectively.

(2) Advantage of CWGAN-TS in Synthetic Data Generation. Fig. 4 shows the synthetic data generation performance of various methods (left number in parentheses). Comparing CWGAN-TS to LSTM, we find that both of them can capture the rising trend of heart rate, but the synthetic data generated by CWGAN-TS is more stable and accurate. Specifically, the performance of LSTM and CWGAN-TS at $t = 21$ (the first synthetic data) are comparable. Subsequently, the synthetic data generated by LSTM tends to fluctuate greatly, resulting in a larger MSE. We posit this is caused by error propagation. As for CWGAN-TS, we see that CWGAN-TS is essentially a combination of LSTMs (see Section 4.2), with the key difference being that CWGAN-TS incorporates an additional GAN loss, but results in more stable synthetic data with a 65% lower MSE than LSTM. This demonstrates **the effectiveness of the GAN loss in mitigating error propagation**. Interestingly, the LSTM has 3.5K parameters while CWGAN-TS has only 3K parameters.

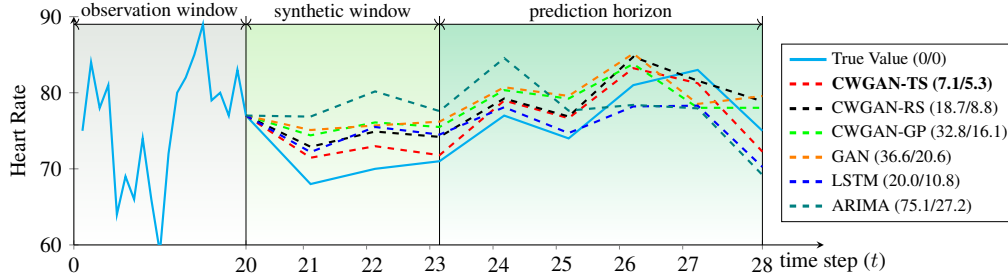


Figure 4: Synthetic data generated by various models and their corresponding forecasting performance using Vital Sign dataset. The values in parentheses are the MSE of synthetic data generation and forecasting performance, averaged over the synthetic window and prediction horizon, respectively.

When comparing CWGAN-TS to CWGAN-GP, we find that the squared error penalty term in (4) significantly improves generation performance (i.e., 78%), suggesting the crucial role of the error penalty term. Moreover, when comparing CWGAN-TS to CWGAN-RS, the experimental results show that the ITC algorithm improves generation performance by 62%, indicating its effectiveness in selecting representative units. Comparing to the original GAN, CWGAN-TS improves generation performance by 81%. We posit this is because CWGAN-TS uses Wasserstein distance as part of the loss function, leading to a more stable learning process.

(3) Forecasting Performance. Fig. 4 also shows the forecasting performance (right number in parentheses). As expected, the model that generates more accurate synthetic data tends to have better forecasting performance (e.g., CWGAN-TS has 40% over CWGAN-RS), suggesting the important role of the CWGAN-TS and the ITC algorithm in improving long-range forecasting. Lastly, similar performance trends are observed for other subjects (see Fig. 5 in the Appendix).

(4) Averaged Performance over All Subjects. We also study the performance averaged over all subjects. In addition to the classical models, the five selected SOTA baselines and a SOTA GAN based model called TimeGAN [47] are also examined. We summarize the average performance in Table 8 in the Appendix, where we observe that CWGAN-TS outperforms benchmarks by up to 10% in synthetic data generation and long-range forecasting.

5 Reflections

In this paper, we propose a competitive long-range forecasting strategy, called GenF, which is able to better balance the forecasting bias and variance, leading to an improvement of 5% - 11% in forecasting performance while having 15% - 50% less parameters. We now conclude the paper by discussing some relevant points and avenues for future research.

(1) Selection of the Synthetic Window Length L : The performance of GenF depends on the choice of L . Our results suggest that as the prediction horizon grows, increasing L could be helpful (i.e., $L = 3$ for $t + 8$, $L = 6$ for $t + 12$ in Table 1). Theoretically determining the optimal L clearly deserves deeper thought. Alternatively, L can be thought of as a hyper-parameter and tuned via trial and error.

(2) Flexibility of GenF: In fact, GenF can be considered as a general framework and is flexible enough to support any model as the synthetic data generator and predictor. We evaluate the forecasting performance using Informer/LogSparse as the predictor and find the performance is not comparable to that of GenF which uses the canonical transformer (see Table 10 in the Appendix). We posit this is due to the simplification of transformer complexity introduced by Informer/LogSparse.

(3) The ITC Algorithm: In the ITC algorithm, we only use first order mutual information as the scoring function. We note that other types of scoring functions, such as joint mutual information, conditional mutual information or pairwise mutual information, could be a better choice for the scoring function. We will explore them in our future research.

(4) PICV and TSCV: We note that our cross validation (CV) method of doing random train-test split at the unit level is known as Population-Informed CV (PICV). PICV is practical as it requires no prior knowledge about the unseen data. We understand that PICV may cause data leakage as there may be correlations across different units. Thus, we examine Time Series CV (TSCV) which

splits the data in chronological order. Our results on the Air Quality dataset demonstrate that for TSCV, GenF remains competitive and outperforms SOTA methods by at least 7.8% (see Table 9 in the Appendix).

(5) Broader Impact: There are several unintended consequences to long-range forecasting. These primarily include the economic and societal impacts of long-range forecasts. For example, a far in the future forecast of CO₂ levels could impact current carbon policies, e.g., the implementation of a carbon tax. Given the influence of long-range forecasting, researchers must try to expose inherent biases in their algorithms, as well as look out for malicious use of algorithms by bad actors.

References

- [1] Martin Arjovsky *et al.* Wasserstein generative adversarial networks. In *ICML*, volume 70, pages 214–223, 2017.
- [2] Alexis Bellot, Kim Branson, and Mihaela van der Schaar. Neural graphical modelling in continuous-time: consistency guarantees and algorithms. In *ICLR*, 2021.
- [3] Alexis Bellot and Mihaela Van Der Schaar. Policy analysis using synthetic controls in continuous-time. In *ICML*, pages 759–768, 2021.
- [4] Gianluca Bontempi *et al.* Machine learning strategies for time series forecasting. In *eBISS*, pages 62–77. Springer, 2012.
- [5] George E. P. Box *et al.* Distribution of residual autocorrelations in autoregressive-integrated moving average time series models. *J. Am. Stat. Assoc.*, 65(332):1509–1526, 1970.
- [6] Jiezhong Cheng *et al.* Towards better forecasting by fusing near and distant future visions. In *AAAI*, pages 3593–3600, 2020.
- [7] Edward Choi *et al.* Using recurrent neural network models for early detection of heart failure onset. *J. Am. Med. Inform. Assoc.*, 24(2):361–370, 2016.
- [8] Thomas M. Cover and Joy A. Thomas. *Elements of Information Theory, 2nd edition*. John Wiley & Sons, 2006.
- [9] Dheeru Dua and Casey Graff. UCI machine learning repository, 2017.
- [10] Zhao *et al.* Bias and generalization in deep generative models: An empirical study. *Neurips*, 31, 2018.
- [11] R. Mohammadi Farsani and E Pazouki. A transformer self-attention model for time series forecasting. *Journal of Electrical and Computer Engineering Innovations (JECEI)*, 9(1):1–10, 2021.
- [12] Maayan Frid-Adar *et al.* GAN-based synthetic medical image augmentation for increased CNN performance in liver lesion classification. *Neurocomputing*, 321:321–331, 2018.
- [13] Ian Goodfellow *et al.* Generative adversarial nets. In *Neurips*, 2014.
- [14] Ishaan Gulrajani *et al.* Improved training of wasserstein gans. In *Neurips*, 2017.
- [15] Sepp Hochreiter and Jürgen Schmidhuber. Long short-term memory. *Neural computation*, 9(8):1735–1780, 1997.
- [16] Mengxiao Hu and Jinlong Li. Exploring bias in gan-based data augmentation for small samples. *arXiv preprint arXiv:1905.08495*, 2019.
- [17] Daniel Jarrett *et al.* Clairvoyance: A pipeline toolkit for medical time series. In *ICLR*, 2021.
- [18] Alistair Johnson *et al.* MIMIC-III clinical database. *PhysioNet*, 2016.
- [19] Diederik P. Kingma and Jimmy Ba. Adam: A method for stochastic optimization. *arXiv preprint arXiv:1412.6980*, 2014.
- [20] Nikita Kitaev *et al.* Reformer: The efficient transformer. In *ICLR*, 2020.
- [21] Alexander Kraskov *et al.* Estimating mutual information. *Physical Review E*, 69(6):066–138, 2004.
- [22] Guokun Lai *et al.* Modeling long-and short-term temporal patterns with deep neural networks. In *ACM SIGIR*, pages 95–104, 2018.
- [23] Vincent LE GUEN and Nicolas THOME. Shape and time distortion loss for training deep time series forecasting models. In *Neurips*, volume 32, 2019.

- [24] Shiyang Li *et al.* Enhancing the locality and breaking the memory bottleneck of transformer on time series forecasting. In *Neurips*, 2019.
- [25] Bryan Lim and Stefan Zohren. Time-series forecasting with deep learning: a survey. *Philosophical Transactions of the Royal Society A*, 379(2194):20200209, 2021.
- [26] Bryan Lim *et al.* Temporal fusion transformers for interpretable multi-horizon time series forecasting. *International Journal of Forecasting*, 37(4):1748–1764, 2021.
- [27] Massimiliano Marcellino *et al.* A comparison of direct and iterated multistep ar methods for forecasting macroeconomic time series. *Journal of econometrics*, 135(1-2):499–526, 2006.
- [28] Filip Milojkovic. Gem house opendata: German electricity consumption in many households over three years 2018-2020 (fresh energy). *IEEE Dataport*, 2021.
- [29] Mehdi Mirza and Simon Osindero. Conditional generative adversarial nets. *arXiv preprint arXiv:1411.1784*, 2014.
- [30] Olof Mogren. C-RNN-GAN: Continuous recurrent neural networks with adversarial training. *arXiv preprint arXiv:1611.09904*, 2016.
- [31] Hanh H. Nguyen *et al.* Multiple neural networks for a long term time series forecast. *Neural Computing & Applications*, 13(1):90–98, 2004.
- [32] Syama Sundar Rangapuram *et al.* Deep state space models for time series forecasting. *Neurips*, 31:7785–7794, 2018.
- [33] Omer Sezer *et al.* Financial time series forecasting with deep learning: A systematic literature review: 2005–2019. *Applied soft computing*, 90:106181, 2020.
- [34] Antti Sorjamaa *et al.* Methodology for long-term prediction of time series. *Neurocomputing*, 70(16-18):2861–2869, 2007.
- [35] Kamile Stankeviciute, Ahmed M. Alaa, and Mihaela van der Schaar. Conformal time-series forecasting. In *Neurips*, volume 34, pages 6216–6228, 2021.
- [36] Ilya Sutskever *et al.* Sequence to sequence learning with neural networks. In *Neurips*, pages 3104–3112, 2014.
- [37] Souhaib Ben Taieb and Amir F. Atiya. A bias and variance analysis for multistep-ahead time series forecasting. *IEEE Trans. Neural. Netw. Learn. Syst.*, 27(1):62–76, 2015.
- [38] Souhaib Ben Taieb *et al.* *Recursive and direct multi-step forecasting: the best of both worlds*. Citeseer, 2012.
- [39] Souhaib Ben Taieb *et al.* A review and comparison of strategies for multi-step ahead time series forecasting based on the nn5 forecasting competition. *Expert Syst. Appl*, 39(8):7067–7083, 2012.
- [40] Binh Tang and David S Matteson. Probabilistic transformer for time series analysis. *Neurips*, 34:23592–23608, 2021.
- [41] José F Torres *et al.* Deep learning for time series forecasting: a survey. *Big Data*, 9(1):3–21, 2021.
- [42] Flunkert Valentin *et al.* Deepar: Probabilistic forecasting with autoregressive recurrent networks. *arXiv preprint:1704.04110*, 2017.
- [43] Ashish Vaswani *et al.* Attention is all you need. In *Neurips*, pages 5998–6008, 2017.
- [44] WorldBank. Electricity & fossil fuel energy consumption. *World Development Indicator*, 2019.
- [45] Neo Wu *et al.* Deep transformer models for time series forecasting: The influenza prevalence case. *arXiv preprint arXiv:2001.08317*, 2020.
- [46] Sifan Wu *et al.* Adversarial sparse transformer for time series forecasting. *Neurips*, 33:17105–17115, 2020.
- [47] Jinsung Yoon *et al.* Time-series generative adversarial networks. In *Neurips*, pages 5508–5518, 2019.
- [48] Rose Yu *et al.* Long-term forecasting using tensor-train rnns. *ArXiv Preprint:1711.00073*, 2017.
- [49] Haoyi Zhou *et al.* Informer: Beyond efficient transformer for long sequence time-series forecasting. *AAAI*, 35(12), 2021.

A Proofs of Theoretical Results

For Proposition 1, we provide minor corrections, which lead to minor changes in the Theorem 1 and Corollary 1, and are described below. Note that these corrections do not alter the form and implications of the results and their discussion in the main paper.

Proposition 1. *Let S be the sum of bias and variance terms, we have $S_{dir} = B_{dir}(N) + V_{dir}(N)$ for direct forecasting and $S_{iter} = B_{iter}(N) + V_{iter}(N)$ for iterative forecasting. For GenF, let $Y_{M-L} = \{X_{L+1}, \dots, X_M\}$ and $Y_L = \{X_{M+1}, \dots, X_{M+L}\}$ be the past observations and let $\tilde{Y}_L = \{\tilde{X}_{M+1}, \dots, \tilde{X}_{M+L}\}$ be the generated synthetic data for the next L time steps. Let $\gamma(\theta, N-L) = f(\{Y_{M-L}, \tilde{Y}_L\}, \theta, N-L) - f(\{Y_{M-L}, Y_L\}, \theta, N-L)$. Note that $\gamma(\theta, 0) = \tilde{Y}_N - Y_N$. We then have,*

$$S_{GenF} = \underbrace{\mathbb{E}_{\theta \sim \Theta, Y}[\gamma(\theta, N-L)^2]}_{\text{Iterative Forecasting}} + \underbrace{B_{dir}(N-L) + V_{dir}(N-L)}_{\text{Direct Forecasting}}, \quad (6)$$

where $\mathbb{E}_{\theta \sim \Theta}[\gamma(\theta, 0)^2] = S_{iter} = B_{iter}(N) + V_{iter}(N)$.

Proof. We consider the decomposition mean-squared error at the horizon N , neglecting the noise term $Z(N)$, as follows

$$\mathbb{E}_{Y, \theta}[(\tilde{X}_{M+N} - X_{M+N})^2] = \mathbb{E}_{Y, \theta}[(f(\{Y_{M-L}, \tilde{Y}_L\}, \theta, N-L) - X_{M+N})^2] \quad (7)$$

$$= \mathbb{E}_Y[(f(\{Y_{M-L}, \tilde{Y}_L\}, \theta, N-L) - (f(\{Y_{M-L}, Y_L\}, \theta, N-L) + (f(\{Y_{M-L}, Y_L\}, \theta, N-L) - X_{M+N}))^2] \quad (8)$$

$$= \mathbb{E}_{Y, \theta}[(f(\{Y_{M-L}, \tilde{Y}_L\}, \theta, N-L) - (f(\{Y_{M-L}, Y_L\}, \theta, N-L))] + \mathbb{E}_{Y, \theta}[(f(\{Y_{M-L}, Y_L\}, \theta, N-L) - X_{M+N})^2] \quad (9)$$

$$= \mathbb{E}_{\theta \sim \Theta, Y}[\gamma(\theta, N-L)^2] + B_{dir}(N-L) + V_{dir}(N-L). \quad (10)$$

Here, the third step follows from the fact that the error terms $f(\{Y_{M-L}, \tilde{Y}_L\}, \theta, N-L) - f(\{Y_{M-L}, Y_L\}, \theta, N-L)$ and $f(\{Y_{M-L}, Y_L\}, \theta, N-L) - X_{M+N}$ are independent, as $f(\{Y_{M-L}, \tilde{Y}_L\}, \theta, N-L) - f(\{Y_{M-L}, Y_L\}, \theta, N-L)$ depends primarily on the error of the iterative forecaster, which is independent of the direct forecasting error. \square

Theorem 1. *We consider the direct forecasting with parameters θ_D , iterative forecasting with parameters θ_I , and the proposed GenF in Proposition (1). Assume that the ground truth realization of the forecasting process can be modelled by some θ_D^* and θ_I^* , and after training, the estimated parameters follow $\theta_D \sim \mathcal{N}(\theta_D^*, \sigma_D^2)$ and $\theta_I \sim \mathcal{N}(\theta_I^*, \sigma_I^2)$. Assume that the iterative forecasting function is 2nd-order L_1, L_2 -Lipschitz continuous, and the direct forecasting function is first order Lipschitz continuous. Let us denote quadratic recurrence relations of the form $b_\alpha(k+1) = b_\alpha(k)(L_1 + 1 + b_\alpha(k)L_2)$, where $b_\alpha(1) = \alpha\sigma_I^2$, for any $\alpha \geq 0$. Assume that iterative forecasting has zero variance and direct forecasting has zero bias. Then, for some constants $\beta_0, \beta_1, \beta_2 \geq 0$, which represent the Lipschitz constants of the direct forecasting function, we have $S_{dir} \leq U_{dir}$, $S_{iter} \leq U_{iter}$ and $S_{GenF} \leq U_{GenF}$, where $U_{dir} = (N-1)\beta_1 + \sigma_D^2\beta_2$, $U_{iter} = b_\alpha(N)^2$, and $U_{GenF} = b_\alpha(L)^2(\beta_0) + (N-L-1)\beta_1 + \sigma_D^2\beta_2$. The quantities α and $\beta_0, \beta_1, \beta_2$ depend on the iterative and direct forecasting functions respectively.*

Proof. Let $X_{k:m} = \{X_k, X_{k+1}, \dots, X_m\}$. Let f_I and f_D represent the iterative and direct forecasting functions respectively, with θ_I and θ_D as their respective parameters. As stated in the theorem, we assume that the ground truth realization can be expressed via some configuration of both these forecasters. That is, if

$$X_{k+1} = f_{GT}(X_{k+1-m:k+1}) + \epsilon \quad (11)$$

represent the ground truth realization that generates the data, and for the direct forecasting function with a horizon N , let

$$\mathbb{E}_\epsilon[X_{k+N}] = f_{GT}(X_{k+1-m:k+1}, N) \quad (12)$$

represent the mean-squared error minimizing function. Then, as per the assumptions stated in the theorem, there exist θ_I^* and θ_D^* such that $f_I(X_{k+1-m:k+1}, \theta_I) \approx f_{GT}(X_{k+1-m:k+1})$ and $f_D(X_{k+1-m:k+1}, N, \theta_D) \approx f_{GT}(X_{k+1-m:k+1}, N)$. Thus, we assume that the direct and iterative forecasters are complex enough to have a configuration close to the ground truth realization. Also note that, as we are only estimating S_{GenF} , we do not consider the noise term in our estimation.

With this, we first estimate the bias of the iterative forecasting part of GenF. First, as θ_I^* represents the underlying realization of the process, we have that

$$X_{m+1} = f_I(X_{1:m}, \theta_I^*) + \epsilon_1, \quad (13)$$

and so on for all subsequent observations, for some $\epsilon_1 \sim \mathcal{N}(0, \sigma_0^2)$. As we assume iterative forecasters with low variance, we intend to compute $(\mu_{m+k} - \hat{\mu}_{m+k})^2$, as the variance term is assumed to be insignificant compared to bias. For the trained f_I with parameters $\theta_I \sim \mathcal{N}(\theta_I^*, \sigma_I^2)$. For the predicted sequence we can write,

$$\hat{X}_{m+1} = f_I(X_{1:m}, \theta_I) + \epsilon'_1 \quad (14)$$

$$\hat{X}_{m+2} = f_I(\{X_{2:m}, \hat{X}_{m+1}\}, \theta_I) + \epsilon'_2, \quad (15)$$

and similarly for the subsequent time-steps. Note that as the only change in the trained realization is in θ_I , the error term ϵ_2 will not change in its distribution, i.e., $\epsilon_2 \sim \mathcal{N}(0, \sigma_0^2)$. We consider a first-order Lipschitz continuous expansion of f_I w.r.t θ_I and a second-order expansion w.r.t the data points X , as we will see that $\mu_{m+k} - \hat{\mu}_{m+k}$ is only affected by the second-order Lipschitz term. For simplicity of notation, we only include the first and second order Taylor expansions of the arguments of f_I in our equations, and write up to the second-order Taylor expansions of all terms. Note that this does not change the 2nd-order Lipschitz continuity constraint. We can then write

$$\hat{X}_{m+2} = f_I(\{X_{2:m}, \hat{X}_{m+1}\}, \theta_I) + \epsilon'_2 \quad (16)$$

$$= f_I(\{X_{2:m}, f_I(X_{1:m}, \theta_I) + \epsilon'_1 + a_1 \mathbb{E}[(\theta_I - \theta_I^*)]\}, \theta_I) + \epsilon'_2 \quad (17)$$

$$= f_I(\{X_{2:m}, f_I(X_{1:m}, \theta_I) + \epsilon'_1\}, \theta_I) + L_1^2 \mathbb{E}[(\theta_I - \theta_I^*)] + L_2 L_1^2 \mathbb{E}[(\theta_I - \theta_I^*)^2] + \epsilon'_2 \quad (18)$$

Here, the notation $\mathbb{E}[(\theta_I - \theta_I^*)]$ and $\mathbb{E}[(\theta_I - \theta_I^*)^2]$ represent the sum and the sum of squares of the differences between the corresponding parameters. As $\theta_I \sim \mathcal{N}(\theta_I^*, \sigma_I^2)$, we have that

$$\hat{\mu}_{m+2} = \mathbb{E}_{\theta_I, X} [f_I(\{X_{2:m}, f_I(X_{1:m}, \theta_I) + \epsilon'_1\}, \theta_I) + L_1^2 \mathbb{E}[(\theta_I - \theta_I^*)] + L_2 L_1^2 \mathbb{E}[(\theta_I - \theta_I^*)^2] + \epsilon'_2] \quad (19)$$

$$\leq \mathbb{E}_{\theta_I, X} [f_I(\{X_{2:m}, f_I(X_{1:m}, \theta_I) + \epsilon'_1\}, \theta_I) + \epsilon'_2] + L_1^2 \mathbb{E}_{\theta_I, X} [\mathbb{E}[(\theta_I - \theta_I^*)]] \\ + L_2 L_1^2 \mathbb{E}_{\theta_I, X} [\mathbb{E}[(\theta_I - \theta_I^*)^2]] \quad (20)$$

$$= \mu_{m+2} + 0 + L_2 L_1^2 \sigma_I^2. \quad (21)$$

Due to the assumption of low-variance iterative forecasters, all subsequent 2nd-order Taylor terms in the expansion of the arguments \hat{X}_{m+i} will be significantly greater than the first order terms. Thus from $m+2$ and onwards, we can substitute the \hat{X}_{m+i} argument of f_I with $\hat{\mu}_{m+i}$, when estimating $\hat{\mu}_{m+3}, \hat{\mu}_{m+4}, \dots$ and so on. Let $\alpha = L_2 L_1^2$. With these considerations, for $\hat{\mu}_{m+3}$, we can write

$$\hat{\mu}_{m+3} = \mathbb{E}_{\theta_I, X} [f_I(\{X_{3:m}, f_I(X_{1:m}, \theta_I) + \epsilon'_1 + L_1 \mathbb{E}[(\theta_I - \theta_I^*)], \mu_{m+2} + \alpha \mathbb{E}[(\theta_I - \theta_I^*)^2]\}, \theta_I) + \epsilon'_2] \quad (22)$$

$$\leq \mathbb{E}_{\theta_I, X} [f_I(\{X_{3:m}, f_I(X_{1:m}, \theta_I) + \epsilon'_1, \mu_{m+2} + \alpha \mathbb{E}[(\theta_I - \theta_I^*)^2]\}, \theta_I) + L_1^2 \mathbb{E}[(\theta_I - \theta_I^*)] \\ + L_2 L_1^2 \mathbb{E}[(\theta_I - \theta_I^*)^2] + L_1 \alpha \mathbb{E}[(\theta_I - \theta_I^*)^2] + L_2 (\alpha \mathbb{E}[(\theta_I - \theta_I^*)^2])^2 + \epsilon'_2] \quad (23)$$

$$\leq \mathbb{E}_{\theta_I, X} [f_I(\{X_{3:m}, f_I(X_{1:m}, \theta_I) + \epsilon'_1, \mu_{m+2} + \alpha \mathbb{E}[(\theta_I - \theta_I^*)^2]\}, \theta_I) + 0 + \\ + \alpha \sigma_I^2 + L_1 \alpha \sigma_I^2 + L_2 (\alpha \sigma_I^2)^2 + \epsilon'_2] \quad (24)$$

$$\leq \mu_{m+3} + \alpha \sigma_I^2 (1 + L_1) + L_2 (\alpha \sigma_I^2)^2 \quad (25)$$

Using this expansion, we can converge to a generalization of the iterative sequence that generates μ_{m+i} , as follows. Let $b_\alpha(i) = \hat{\mu}_{m+i} - \mu_{m+i}$. Based on our previous expansions, note that we can write:

$$b_\alpha(k+1) = (1 + L_1) b_\alpha(k) + L_2 (b_\alpha(k))^2 \quad (26)$$

Here, (26) represents a quadratic recurrence function and using the same we note that the bias term for f_I , $(\hat{\mu}_{m+L} - \mu_{m+L})^2$, can then be written as $(\hat{\mu}_{m+L} - \mu_{m+L})^2 \leq b_\alpha(L)^2$. This accounts for the error for the iterative part of GenF. Next, we first estimate the variance of the direct forecasting function f_D . We have that

$$V_{dir}(N-L) = \mathbb{E}_{X, \theta_D} \left[\left(f_D(X_{L:m+L}, \theta_D, N-L) - \mathbb{E}_{\theta_D \sim \mathcal{N}(\theta_D^*, \sigma_D^2)} [f_D(X_{L:m+L}, \theta_D, N-L)] \right)^2 \right]. \quad (27)$$

As we assume low-bias f_D , the mean estimate $\mathbb{E}_{\theta_D \sim \mathcal{N}(\theta_D^*, \sigma_D^2)} [f_D(X_{L:m+L}, \theta_D, N-L)] = f_D(X_{L:m+L}, \theta_D^*, N-L)$, yielding

$$\mathbb{E}_{X, \theta_D \sim \mathcal{N}(\theta_D^*, \sigma_D^2)} \left[\left(f_D(X_{L:m+L}, \theta_D, N-L) - f_D(X_{L:m+L}, \theta_D^*, N-L) \right)^2 \right]. \quad (28)$$

Using the Lipschitz continuity of f_D w.r.t θ_D (assuming a Lipschitz constant of β_2), and the Lipschitz continuity of $V_{dir}(N-L)$ w.r.t $N-L$ itself (Lipschitz constant of β_1), we can write

$$V_{dir}(N-L) \leq V_{dir}(1) + (N-L-1)\beta_1 \quad (29)$$

$$= \mathbb{E}_{X, \theta_D \sim \mathcal{N}(\theta_D^*, \sigma_D^2)} \left[(f_D(X_{L:m+L}, \theta_D, 1) - f_D(X_{L:m+L}, \theta_D^*, 1))^2 \right] + (N-L-1)\beta_1 \quad (30)$$

$$\leq \beta_2 \mathbb{E}_{\theta_D \sim \mathcal{N}(\theta_D^*, \sigma_D^2)} \left[(\theta_D - \theta_D^*)^2 \right] + (N-L-1)\beta_1 = \beta_2 \sigma_D^2 + (N-L-1)\beta_1. \quad (31)$$

Note that we use this two-step Lipschitz decomposition, instead of a single-step decomposition with θ_D , as without any constraints on the horizon $N-L$, the Lipschitz constant of $f_D(X_{L:m+L}, \theta_D, N-L)$ w.r.t θ_D , as $N-L \rightarrow \infty$, will be very large and thus, vacuous. Through this two-step decomposition, note that the Lipschitz constant β_2 will not be as large, as it applies to $f_D(X_{L:m+L}, \theta_D, 1)$ which has a horizon of 1. Next, we bound the last term $\mathbb{E}_{\theta \sim \Theta} [\gamma(\theta, N-L)^2]$ in Proposition 1, again via the Lipschitz continuity of $f(\{X_{L:m}, \tilde{X}_{m:m+L}\}, \theta, N-L)$ w.r.t $\{X_{L:m}, \tilde{X}_{m:m+L}\}$ (assuming a Lipschitz constant of β'_0), as follows.

$$\begin{aligned} \mathbb{E}_{\theta \sim \Theta} [\gamma(\theta, N-L)^2] &= \mathbb{E}_{\theta \sim \mathcal{N}(\theta_D^*, \sigma_D^2)} \left[\left(f(\{X_{L:m}, \tilde{X}_{m:m+L}\}, \theta, N-L) \right. \right. \\ &\quad \left. \left. - f(\{X_{L:m}, X_{m:m+L}\}, \theta, N-L) \right)^2 \right] \end{aligned} \quad (32)$$

$$\leq \mathbb{E}_{\theta \sim \mathcal{N}(\theta_D^*, \sigma_D^2)} \left[\left(L\beta'_0(\tilde{X}_{m+L} - X_{m+L}) \right)^2 \right] \quad (33)$$

$$\leq (L\beta'_0)^2 \mathbb{E}_{\theta \sim \mathcal{N}(\theta_D^*, \sigma_D^2)} \left[\left(\tilde{X}_{m+L} - X_{m+L} \right)^2 \right] = (L\beta'_0)^2 (b_\alpha(L))^2. \quad (34)$$

Denoting $\beta_0 = (L\beta'_0)^2$, and combining all error upper bounds from the iterative and direct forecasting functions, we finally have

$$S_{GenF} \leq \beta_0 (b_\alpha(L))^2 + \beta_2 \sigma_D^2 + (N-L-1)\beta_1 = b_\alpha(L)^2 (\beta_0) + (N-L-1)\beta_1 + \sigma_D^2 \beta_2. \quad (35)$$

Denoting this upper bound via U_{GenF} , and similarly for U_{iter} and U_{dir} , yields the final result. \square

Corollary 1. *U_{dir} , U_{iter} and U_{GenF} are as defined in Theorem 1. When $\beta_0 < \min\{\beta_1/b_\alpha(1)^2, (b_\alpha(N)^2 - \sigma_D^2 \beta_2)/b_\alpha(N-1)^2\}$, we have that $U_{GenF} < U_{iter}$ and $U_{GenF} < U_{dir}$, for some $0 < L < N$. Furthermore, when $(N-1)\beta_1 + \sigma_D^2 \beta_2 \approx b_\alpha(N)^2$, we have $U_{GenF} < U_{iter}$ and $U_{GenF} < U_{dir}$, for any choice of $0 < L < N$.*

Proof. First, with regard to the various terms in U_{GenF} , we note that $b_\alpha(L)^2 (\beta_0)$ is an increasing function of L , whereas $(N-L-1)\beta_1 + \sigma_D^2 \beta_2$ is a decreasing function of L . For simplicity of notation, let us denote U_{GenF} via $U_{GenF}(L)$, for a certain choice of L . Thus, for $U_{GenF}(L)$ to be less than the value at its extremes (U_{dir} at $L=0$ and U_{iter} at $L=N$) for some $0 < L < N$, we must have that $U_{dir} - U_{GenF}(1) > 0$ and $U_{iter} - U_{GenF}(N-1) > 0$. This yields

$$\beta_1 - b_\alpha(1)^2 (\beta_0) > 0, \text{ and} \quad (36)$$

$$b_\alpha(N)^2 - b_\alpha(N-1)^2 (\beta_0) - \sigma_D^2 \beta_2 > 0, \quad (37)$$

respectively, which summarizes to $\beta_0 < \min\{\beta_1/b_\alpha(1)^2, (b_\alpha(N)^2 - \sigma_D^2 \beta_2)/b_\alpha(N-1)^2\}$. Furthermore, we note that when the upper bounds at $L=0$ and $L=N$ are equal, i.e., $(N-1)\beta_1 + \sigma_D^2 \beta_2 \approx b_\alpha(N)^2$, then assuming $\beta_0 < \min\{\beta_1/b_\alpha(1)^2, (b_\alpha(N)^2 - \sigma_D^2 \beta_2)/b_\alpha(N-1)^2\}$, we must have that $U_{GenF}(L) < (N-1)\beta_1 + \sigma_D^2 \beta_2$ and $U_{GenF}(L) < b_\alpha(N)^2$ for any $0 < L < N$. \square

B Supplementary Results

In this Appendix, we show some additional experimental results. Specifically,

1. In Section B.1, we present the performance comparison using Multi-Site Air Quality dataset (forecasting NO₂ emissions), the World Energy Consumption dataset (forecasting fossil fuel consumption), the House Electricity Consumption dataset (forecasting electricity consumption) and the Green Gas dataset (forecasting the green gas concentration).
2. In Section B.2, we conduct an ablation study on more subjects and provide the experimental results.
3. In Section B.3, we show the ablation study results averaged on all subjects studied in the MIMIC-III Vital Signs dataset.
4. In Section B.4, we evaluate the performance of GenF using Time Series Cross Validation (TSCV) and compare it to the performance of Population-Informed Cross Validation (PICV)
5. In Section B.5, we examine the forecasting performance of GenF using LogSparse and Informer as the predictor.

B.1 Performance Comparison on Air Quality and Energy Consumption Datasets

In this subsection, we show the performance comparison on the Multi-Site Air Quality dataset (forecasting NO₂ emissions), the World Energy Consumption dataset (forecasting fossil fuel consumption), the House Electricity Consumption dataset (forecasting electricity consumption) and the Green Gas dataset (forecasting the green gas concentration). We follow the same parameter tuning procedure in Section 4.2 and the configurations for GenF and the five SOTA methods are provided in Table 3. The training and test procedures of GenF are summarized in Algorithm 1. The performance comparisons are summarized in Tables 4 - 7.

We can see that the predictive performance largely mirror those in Table 1: the proposed GenF significantly outperforms the three strong baselines (i.e., 4.3% - 11% in Table 4 and 8.3% - 14.7% in Table 5). Furthermore, as the prediction horizon grows, generating more synthetic data tends to provide better forecasting performance. As an example, in Table 4, GenF-2 provides the best predictive performance at $t + 8$ while GenF-5 can obtain the best performance at $t + 15$.

Generative Forecasting (GenF)		
CWGAN-TS		Predictor
Generator	Discriminator	-
$(S, M + 1, K)$	$(S, M + 1, K)$	(S, M, K)
LSTM (5)	LSTM (5)	Atten En (3)
Linear (12)	Linear (12)	Atten En (3)
Linear (K)	Linear (4)	Atten De (3)
Reshape $(S, 1, K)$	Linear (1)	Atten De (3)
-	-	Linear (1)

<p>LSTNet skip-length $p = 5$, gradient clipping = 10, epoch = 1000, dropout = 0.1, batchsize = 64.</p> <p>TLSTM learning rate (lr) decay = 0.8, lr = 1e-3, dropout = 0.1, batchsize = 64, epoch = 1000.</p> <p>DeepAR LSTM (20), embedding size = 10 batchsize = 64, LSTM dropout = 0.1, lr = 1e-3.</p> <p>LogSparse embedding size = 16, kernel size = 9 batchsize = 64, epoch = 1000, lr = 3e-3.</p> <p>Informer Encoder/Decoder Layers = 2, heads = 4 batchsize = 32, dropout = 0.05, lr = 1e-3.</p>
--

Table 3: (left) Network configuration of GenF. The fourth row represents the shape of input variables and the parameter in Linear(·) is the number of output units. The parameter in LSTM(·) is the hidden state size. The parameter in Atten En and Atten De is the number of heads in multi-head encoder and multi-head decoder. (right) The training details of SOTA methods.

Algorithm 1 The Algorithm of Generative Forecasting

- Require:** (i) Time series dataset $\mathbb{D} \in \mathbb{R}^{S \times M \times K}$; (ii) $\lambda, \beta=5, 1$ (see (1)); (iii) batch size = 64; (iv) Adam Optimizer (lr = 0.001).
- 1: Randomly split \mathbb{D} (unit level): training dataset $\mathbb{T} \in \mathbb{R}^{S_1 \times M \times K}$ (60%), i.e., $\mathbb{T} : \{X_1^i, \dots, X_M^i\}$ for $i = 1, \dots, S_1$ and $X \in \mathbb{R}^K$, test dataset $\mathbb{Q} \in \mathbb{R}^{S_2 \times M \times K}$ (20%), validation dataset $\in \mathbb{R}^{S_3 \times M \times K}$ (20%).
 - 2: Apply the ITC algorithm to split \mathbb{T} (unit level): training dataset $\mathbb{H} \in \mathbb{R}^{S_4 \times M \times K}$ (50%), training dataset $\mathbb{P} \in \mathbb{R}^{S_5 \times M \times K}$ (50%).
 - 3: Training dataset $\mathbb{H} \xrightarrow{\text{train}}$ the Generator (G) and Discriminator (D) in CWGAN-TS via loss function (1).
 - 4: **for** $j = 1$ to L **do**
 - 5: (i) Synthetic Data Generation: $G(\mathbb{P}) = \mathbb{Y}_1 \in \mathbb{R}^{S_5 \times 1 \times K}$, i.e., $\mathbb{Y}_1 : \{\bar{X}_{M+j}^i\}$ for $i = 1, \dots, S_5$; $G(\mathbb{Q}) = \mathbb{Y}_2 \in \mathbb{R}^{S_2 \times 1 \times K}$.
 - 6: (ii) Prune the oldest observation: $\mathbb{P} \leftarrow \mathbb{P} \setminus X_j^i$, i.e., $\{X_{j+1}^i, \dots, X_{M+j-1}^i\}$ for $i = 1, \dots, S_5$; $\mathbb{Q} \leftarrow \mathbb{Q} \setminus X_j^i$.
 - 7: (iii) Concatenation: $\mathbb{P} \leftarrow \mathbb{P} \oplus \mathbb{Y}_1$, i.e., $\{X_{j+1}^i, \dots, X_{M+j-1}^i, \bar{X}_{M+j}^i\}$ for $i = 1, \dots, S_5$; $\mathbb{Q} \leftarrow \mathbb{Q} \oplus \mathbb{Y}_2$.
 - 8: **end for**
 - 9: Training Dataset $\mathbb{P} \xrightarrow{\text{train}}$ transformer based Predictor, Testing Dataset $\mathbb{Q} \xrightarrow{\text{test}}$ transformer based Predictor.
 - 10: **Return** MSE, MAE and sMAPE between predicted values and real values.
-

Prediction Horizon	t + 8		t + 12		t + 15		t + 18		
Metrics	MAE	sMAPE	MAE	sMAPE	MAE	sMAPE	MAE	sMAPE	
ARIMA	5.3±0.7	5.9±0.6	7.6±0.5	8.5±0.7	9.2±0.6	11.4±1.1	10.9±0.8	13.5±2.1	
LSTM	4.7±0.5	5.4±0.3	6.8±0.4	7.7±0.8	7.9±0.5	10.1±0.9	9.4±0.6	12.3±1.9	
SOTA	TLSTM	4.2±0.2	5.0±0.3	5.7±0.1	7.3±0.5	6.9±0.3	8.9±1.1	8.2±0.3	10.8±1.7
	LSTNet	4.0±0.1	4.7±0.4	5.2±0.2	6.2±0.8	6.8±0.3	8.7±0.8	7.9±0.3	10.5±1.4
	DeepAR	4.3±0.2	5.1±0.4	5.4±0.3	6.3±0.5	7.1±0.4	9.0±1.0	8.5±0.4	10.9±1.8
	Informer	3.9±0.3	4.6±0.2	4.8±0.2	5.9±0.3	6.4±0.5	8.1±0.8	7.3±0.4	9.4±1.2
	LogSparse	4.1±0.3	4.7±0.5	4.9±0.3	6.1±0.4	6.6±0.2	8.2±0.9	7.6±0.2	9.8±1.5
GenF-2 (Ours)	3.6±0.2	4.4±0.6	4.6±0.2	5.5±0.7	6.1±0.2	7.8±1.2	7.1±0.5	8.9±1.1	
GenF-3 (Ours)	3.6±0.2	4.5±0.4	4.5±0.3	5.4±0.6	5.9±0.3	7.6±1.0	6.8±0.4	8.5±0.8	
GenF-5 (Ours)	3.7±0.2	4.5±0.5	4.6±0.4	5.5±0.4	5.8±0.3	7.5±0.9	6.5±0.3	8.4±0.7	

Table 4: Performance comparison (MAE, sMAPE±standard deviation) between three variants of GenF and two classical models, five SOTA methods in fossil fuel consumption using the World Energy Consumption dataset. Due to the time span of the dataset (from 1971 to 2014), we only show predictive performance up to t + 18. The bold indicates the best performance.

Prediction Horizon	t + 8		t + 12		t + 30		t + 60		
Metrics	MAE	sMAPE	MAE	sMAPE	MAE	sMAPE	MAE	sMAPE	
ARIMA	21.3±1.7	26±6	27.8±1.5	29±9	29.2±2.6	34±11	31.9±1.8	35±9	
LSTM	19.7±1.5	22±3	24.6±1.4	27±8	25.9±1.7	31±9	29.4±3.1	33±6	
SOTA	TLSTM	18.8±1.0	20±5	20.7±1.9	22±8	24.0±2.0	28±9	27.5±2.3	31±9
	LSTNet	17.8±2.0	18±4	19.9±1.8	21±9	23.6±2.2	25±6	27.0±2.5	28±10
	DeerAR	19.2±1.3	21±5	22.4±2.0	25±7	24.3±2.1	29±7	28.2±2.9	30±8
	Informer	18.2±1.4	20±3	20.4±1.2	22±8	23.1±1.9	24±5	26.1±2.5	29±7
	LogSparse	18.1±1.5	20±4	21.5±1.5	24±6	23.5±2.3	26±5	26.7±2.6	29±8
GenF-2 (Ours)	16.3±1.8	16±4	18.0±1.7	19±6	20.5±2.2	23±9	24.2±2.5	27±12	
GenF-3 (Ours)	16.5±1.8	16±5	18.2±2.0	19±4	20.3±2.4	23±8	24.0±2.4	26±9	
GenF-6 (Ours)	16.9±1.3	17±3	18.5±1.9	19±3	19.7±2.0	22±5	22.9±1.8	25±8	

Table 5: Performance comparison (MAE, sMAPE (%)±standard deviation) between three variants of GenF and two classical models, five SOTA methods in predicting NO₂ emission using the Multi-Site Air Quality dataset. The bold indicates the best performance.

Prediction Horizon	t + 8		t + 12		t + 30		t + 60		
Metrics	MAE	sMAPE	MAE	sMAPE	MAE	sMAPE	MAE	sMAPE	
ARIMA	5.0±0.9	6.9±1.0	5.8±1.3	7.7±1.4	9.5±1.6	11.5±1.7	18.9±2.8	25.4±2.9	
LSTM	4.6±0.7	6.3±0.9	5.2±1.1	7.4±1.3	9.0±1.4	11.2±1.6	17.6±2.1	23.6±2.6	
SOTA	TLSTM	4.4±0.6	6.1±0.7	4.9±0.9	7.1±1.0	8.8±1.3	11.0±1.5	16.9±2.3	23.1±2.3
	LSTNet	4.8±0.9	6.4±1.0	5.1±0.8	7.2±1.0	8.7±1.2	10.9±1.4	16.4±2.1	22.7±2.0
	DeerAR	4.7±0.8	6.2±0.9	4.8±0.8	7.0±0.9	8.5±1.0	10.6±1.2	16.1±1.9	22.1±2.0
	Informer	3.8±0.6	5.9±0.8	4.9±1.0	7.1±0.9	8.6±1.4	10.8±1.6	15.3±2.4	19.8±2.7
	LogSparse	4.5±0.5	6.2±0.6	5.2±1.1	7.4±1.2	8.8±1.0	10.9±1.1	15.7±2.0	20.9±1.8
GenF-2 (Ours)	3.6±0.5	5.7±0.6	4.4±0.8	6.6±1.2	8.4±1.2	11.0±2.3	15.2±2.3	19.4±3.0	
GenF-3 (Ours)	3.9±0.8	5.9±0.9	4.6±0.9	6.9±1.1	8.1±1.4	10.6±1.5	14.1±2.0	18.5±2.5	

Table 6: Performance comparison (MAE, sMAPE (%)±standard deviation) between three variants of GenF and two classical models, five SOTA methods in predicting electricity consumption using the House Electricity Consumption dataset. Note that all MAE values are divided by 10¹¹ as the readings are cumulative and large. The bold indicates the best performance.

Prediction Horizon	t + 8		t + 12		t + 30		t + 60		
Metrics	MAE	sMAPE	MAE	sMAPE	MAE	sMAPE	MAE	sMAPE	
ARIMA	6.3±1.2	7.6±0.9	7.1±1.3	8.8±1.4	12.4±1.9	11.2±1.8	13.5±2.2	12.4±2.3	
LSTM	5.9±0.9	7.2±0.7	6.6±1.1	8.1±1.2	11.3±1.4	10.6±1.4	12.1±1.7	11.6±1.9	
SOTA	TLSTM	5.8±0.8	7.0±0.6	6.5±0.9	7.9±1.1	11.0±1.2	10.4±1.2	12.4±1.8	11.8±2.0
	LSTNet	6.0±0.9	6.8±0.5	6.6±1.0	8.1±1.2	11.5±1.6	10.8±1.4	12.6±1.5	11.7±2.1
	DeerAR	6.4±1.0	7.5±0.7	6.3±0.9	7.9±1.0	11.8±1.7	10.6±1.5	11.8±1.6	11.2±1.7
	Informer	5.5±0.6	6.8±0.5	6.3±1.0	8.2±1.1	10.7±1.3	10.1±1.1	11.5±1.5	10.9±1.5
	LogSparse	5.7±0.8	7.0±0.5	6.6±1.1	8.4±1.3	11.4±1.5	10.5±1.3	12.2±1.7	11.4±1.8
GenF-2 (Ours)	5.1±0.6	6.4±0.5	5.8±0.7	7.5±0.8	10.2±1.1	9.6±1.3	11.7±1.6	10.4±1.9	
GenF-5 (Ours)	5.3±0.7	6.6±0.6	5.9±0.8	7.7±0.9	9.4±1.0	9.2±1.1	10.6±1.3	9.9±1.4	

Table 7: Performance comparison (MAE, sMAPE (%)±standard deviation) between three variants of GenF and two classical models, five SOTA methods in predicting greenhouse gas concentrations using the Greenhouse Gas dataset. Note that all MAE values are multiplied by 100. The bold indicates the best performance.

B.2 Ablation Study on More Units

We repeat our ablation study using Subjects ID 109 and 890 in the MIMIC-III Vital Sign dataset. In Fig. 5, we observe that the proposed CWGAN-TS can generate more accurate and stable synthetic data as compared to other studied approaches. The error penalty term and the ITC algorithm can help to improve the performance in generating synthetic data. For example, in the upper figure, when comparing CWGAN-TS to CWGAN-RS, the results demonstrate that the ITC algorithm helps to improve the performance by 34%, indicating its effectiveness in selecting typical units. Compared to the CWGAN-GP, CWGAN-TS improves performance by 80% in generating synthetic data, suggesting the crucial role of the error penalty term. Furthermore, the model that can generate accurate synthetic data tends to have better forecasting performance. This suggests the important role of the CWGAN-TS and the ITC algorithm in improving long-range forecasting.

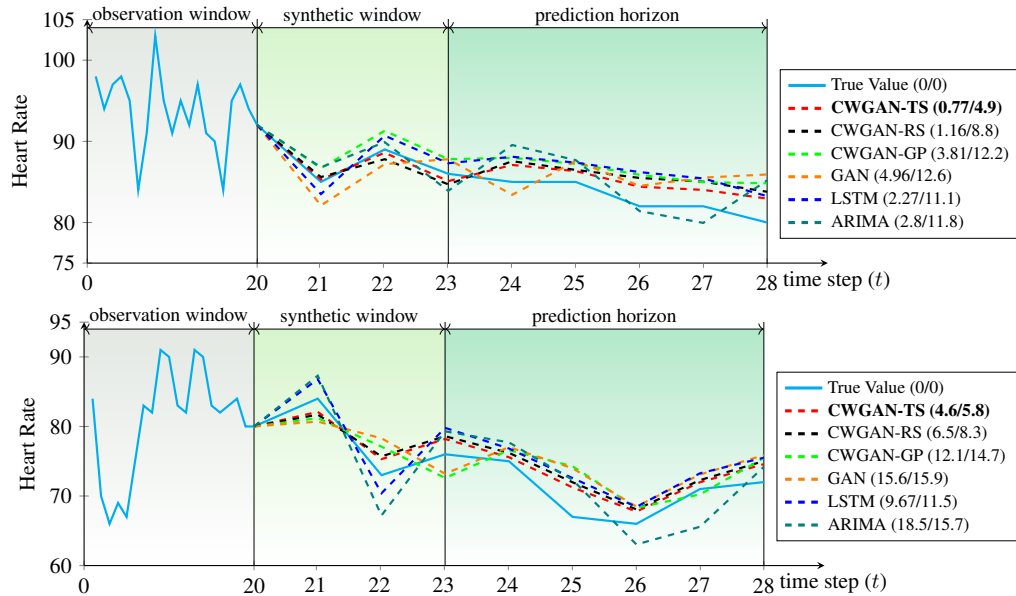


Figure 5: Synthetic data recursively generated by various models and their corresponding forecasting performance based on observed and generated data, for predicting heart rate using the MIMIC-III Vital Signs dataset (Upper: Subject ID 109, lower: Subject ID 890). The values in parentheses are the MSE of the synthetic data generation and the forecasting performance, averaged over the synthetic window and prediction horizon, respectively.

B.3 Ablation Study: Averaged Performance over All Subjects

In this subsection, we study the synthetic data generation performance ($t + 1$ to $t + 3$) and the corresponding forecasting performance ($t + 4$ to $t + 8$) based on observed and synthetic data. Instead of a single subject, we show the averaged performance of all subjects in Table 8. We highlight that the generative performance of CWGAN-TS at $t + 1$ is comparable to or worse than the strong baselines. However, starting from $t + 2$, the generative performance of CWGAN-TS becomes better, leading to better forecasting performance. This demonstrates the superior performance of CWGAN-TS in mitigating error propagation over the strong baselines and its impact on the forecasting performance. Overall, we observe that CWGAN-TS outperforms the best performing benchmark by 5.9% - 6.86% in synthetic data generation and by 5.06% - 10.9% in long-range forecasting.

Performance (MSE)	Generation			Forecasting			
	$t + 1$	$t + 2$	$t + 3$	$t + 4$	$t + 8$	$t + 12$	$t + 24$
ARIMA	106.3	125.7	145.3	160.2	193.2	201.4	225.7
LSTM	95.2	110.6	127.8	142.8	169.6	187.3	199.4
LSTNet	91.3	107.4	116.8	136.8	164.3	179.4	189.3
TLSTM	90.2	106.5	113.2	129.3	159.4	169.8	185.7
DeepAR	90.9	109.4	118.4	134.3	165.8	176.8	193.6
Informer	89.7	105.2	109.4	133.1	155.3	170.7	185.7
LogSparse	89.3	103.7	114.8	135.3	157.2	171.2	181.7
TimeGAN	94.2	114.3	121.8	139.7	167.9	180.4	195.3
CWGAN-TS (Ours)	90.7	97.5	101.9	115.2	145.3	161.2	169.4
Min Improvement	-	5.97%	6.86%	10.9%	6.44%	5.06%	6.77%

Table 8: Ablation Study: Averaged results (MSE) of all subjects in generating/forecasting heart rate using CWGAN-TS and others.

B.4 More Results Using TSCV

We repeated our experiments for predicting NO₂ emission (the Air Quality dataset) using Time Series Cross Validation (TSCV). Specifically, all datasets are split into training set (60%), validation set (20%) and test set (20%) in chronological order to ensure that there is no potential data leakage from using future observations from the other units. We tune all parameters using the validation set (same as Section 4.2) and compare the performance (MSE±standard deviation over 5 runs) of using TSCV to Population Informed Cross Validation (PICV) as follows. We can see that the predictive performance becomes slightly different as the training and test data have changed, but the proposed GenF still outperforms the strong baselines by at least 7.8% (compare GenF-2 to LSTNet at $t + 12$).

Prediction Horizon	PICV			TSCV		
	$t + 4$	$t + 8$	$t + 12$	$t + 4$	$t + 8$	$t + 12$
TLSTM	548±13	867±33	993±23	603±22	819±26	1023±29
LSTNet	518±33	827±28	919±39	557±27	790±25	940±30
DeepAR	562±19	887±24	1047±36	647±26	868±21	1069±35
Informer	534±15	851±23	922±31	585±28	889±20	971±33
LogSparse	543±17	835±25	907±35	572±29	855±19	951±31
GenF-1	465±24	715±31	856±23	509±32	688±25	893±27
GenF-2	409±29	669±27	814±30	433±24	593±29	866±22

Table 9: Performance comparison (MSE±standard deviation) between PICV and TSCV using the Multi-Site Air Quality dataset.

B.5 Flexibility of GenF

The idea of GenF is to balance iterative and direct forecasting using synthetic data. In the main paper, we use CWGAN-TS as the synthetic data generator and the canonical transformer as the predictor. In fact, GenF can be considered as a general framework and is flexible to support any model as the synthetic data generator and the predictor. In Section 4.4, we have examined several variants of CWGAN-TS in synthetic data generation. In this subsection, we use the same CWGAN-TS as the synthetic data generator and replace the canonical transformer with two SOTA transformer based methods: Informer and LogSparse. We let CWGAN-TS generate synthetic data for next 6 time steps and summarize the corresponding forecasting performance (MAE, sMAPE±standard deviation over 3 runs) in Table 10.

It can be seen that the GenF with the canonical transformer as the predictor (denoted as GenF-6*) outperforms the other configurations. We posit this is mainly due to two reasons: (i) Given the long-range dependencies are already captured via the synthetic data, using deep transformer models such as LogSparse and Informer may not be helpful. It is because that these SOTA methods aim to simplify the complexity of the self-attention mechanism and it is essentially a trade-off between performance and complexity, meaning the simplification comes with a loss in performance. (ii) The deep transformer models (e.g., 5 - 7 layers in Informer) may introduce the overfitting issue, leading to poor forecasting performance.

Prediction Horizon	t + 8		t + 12		t + 30		t + 60	
Metrics	MAE	sMAPE	MAE	sMAPE	MAE	sMAPE	MAE	sMAPE
GenF-6-Informer	6.4±0.2	5.3±0.4	7.7±0.6	6.4±0.6	11.4±1.4	9.9±1.4	13.8±2.6	11.4±0.9
GenF-6-LogSparse	6.6±0.5	5.6±0.4	8.0±0.4	6.7±0.5	11.7±1.2	9.7±0.8	14.7±2.9	11.5±1.4
GenF-6* (Ours)	6.3±0.4	5.2±0.3	7.4±0.7	6.2±0.6	10.7±1.1	8.9±0.9	12.6±2.5	10.2±1.4

Table 10: Performance (MAE, sMAPE±standard deviation) of predicting blood pressure using the MIMIC-III dataset. All methods use CWGAN-TS to generate synthetic data for next 6 time steps. GenF-6-Informer is to use Informer as the predictor, GenF-6-LogSparse is to use LogSparse as the predictor and GenF-6* is to use the canonical transformer as the predictor.